Metastable states of Si^- observed in a cryogenic storage ring

D. Müll,[1] F. Grussie,[1] K. Blaum,[1] S. George,[1,2] J. Göck,[1] M. Grieser,[1] R. von Hahn,[1] Z. Harman,[1] Á. Kálosi,[1] C. H. Keitel,[1] C. Krantz,[1] C. Lyu,[1] O. Novotný,[1] F. Nuesslein,[1] D. Paul,[1] V. C. Schmidt,[1] S. Singh,[1] S. Sunil Kumar,[1,*] X. Urbain,[3] A. Wolf,[1] and H. Kreckel[1,†]

[1]*Max-Planck-Institut für Kernphysik, 69117 Heidelberg, Germany*

[2]*Institut für Physik, Universität Greifswald, 17487 Greifswald, Germany*

[3]*Institute of Condensed Matter and Nanosciences, Université Catholique de Louvain, Louvain-la-Neuve B-1348, Belgium*

(Received 17 May 2021; accepted 9 August 2021; published 8 September 2021)

We have used the Cryogenic Storage Ring (CSR) at the Max Planck Institute for Nuclear Physics to study long-lived metastable states of the silicon anion. A Si^- beam of 58 keV kinetic energy was stored in the ultrahigh cryogenic vacuum of the CSR, employing only electrostatic deflection elements. We used laser systems at various wavelengths to infer information on the decay of the metastable anionic states by selective photodetachment. Our results give evidence of an excited anionic state for which we determine the extremely long lower lifetime limit of 5.7 h at 90% confidence level, consistent with theoretical predictions for the ^2D term. Furthermore, we find an average lifetime of $\tau = (22.2 \pm 2.5)$ s for the weakly bound ^2P states, employing coincidence counting with a pulsed nanosecond laser at 2.45 μm. Using a laser depletion technique, we produce a pure ground term $^4S_{3/2}$ Si^- beam, and we quantify the fraction of ions in metastable states in our initial ion sample. We combine our experimental efforts with state-of-the-art multiconfiguration Dirac-Hartree-Fock calculations for the radiative lifetimes of all metastable levels of Si^-. We find these calculations to be in excellent agreement with our measurements and to improve previous efforts considerably.

DOI: 10.1103/PhysRevA.104.032811

I. INTRODUCTION

Negative ions are excellent benchmark systems to study the electronic structure in atomic physics. The comparatively shallow potential formed by polarization forces between the neutral atom and the extra electron is particularly sensitive to correlation effects among the electrons. Most of the information we have on negative ions has been inferred from experiments that detach the outer electron by either particle or photon impact [1]. In this framework, energy-resolved experiments can shed light on the electron affinity and the detachment behavior at threshold.

Experimental data on excited state lifetimes are much more sparse. As few negative ions have electric dipole-allowed $E1$ transitions between bound anionic states (notable exceptions being Os^- [2,3], Ce^- [4], La^- [5,6], and Th^- [7], which have attracted attention as possible candidates for laser cooling of negative ions [3,5–11]), the decay of metastable states usually proceeds through electric-dipole forbidden magnetic dipole $M1$ or electric quadrupole $E2$ transitions. Consequently, anionic excited states can exhibit extremely long lifetimes, which is a challenge for experimental studies. As the absence of strong $E1$ transitions also inhibits the use of spectroscopic or fluorescence-based detection schemes, the method of choice relies on storing negative ions in ion-beam traps or storage rings and the detection of neutral daughter products following a detachment process. The proof-of-principle case for these types of experiments has been the experimental determination of the lifetime of metastable He^- ions. Helium does not form stable anions, but it features several metastable states, with the most long-lived level ($1s2s2p\ ^4P_{5/2}$) undergoing autodetachment with a lifetime of 359 μs [12]. To attain a precise value, it took an electrostatic and cryogenic ion-beam trap to avoid both magnetic mixing effects of the sublevels as well as photodetachment by ambient black-body radiation (see [12–14] and references therein). These measurements demonstrated the potential of modern electrostatic storage devices for lifetime measurements of negative ions.

Metastable state lifetimes for the $4p^5\ ^2P_{1/2}$ and $5p^5\ ^2P_{1/2}$ levels of Se^- and Te^-, respectively, were determined at the magnetic CRYRING in Stockholm. These lifetimes were of the order of a few seconds [16]. More recently, the lifetimes of the $3p^5\ ^2P_{1/2}$ level in $^{32}S^-$ and the $3d^8\ ^2D_{3/2}$ level in Ni^- were measured to be (503 ± 53) s [17] and (15.1 ± 0.4) s [18], respectively, at the electrostatic cryogenic storage ring DESIREE [19]. Very recently, the same facility was used to observe two metastable states in Ir^-, which were found to

*Present address: Department of Physics and Center for Atomic, Molecular, and Optical Sciences and Technologies, Indian Institute of Science Education and Research (IISER) Tirupati, Tirupati 517507, Andhra Pradesh, India.

†Corresponding author: holger.kreckel@mpi-hd.mpg.de

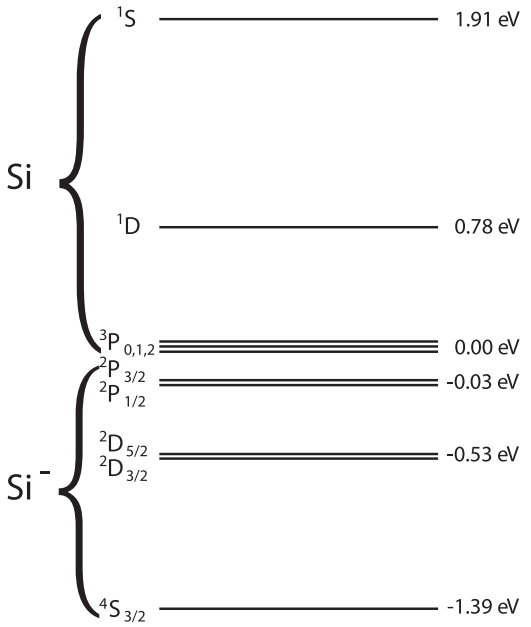

FIG. 1. Level diagram (energy axis not to scale) for Si^- and the relevant neutral levels. The level energies are given with respect to the neutral $^3P_0$ ground state. The fine-structure states of the neutral ground term increase in energy with increasing J quantum number [15]. The ordering of the anionic ^2P fine-structure states has—to the best of our knowledge—not been resolved experimentally. The energetic order plotted here is based on our calculations described in Sec. II, where details on the energies and level splittings of the negative states can be found.

have lifetimes around ∼133 ms and ∼172 ms [20]. In particular the long-lived example of metastable S^- demonstrates that the advent of next-generation cryogenic instruments opens up a completely different regime for lifetime measurements of long-lived anionic states.

Here we report a combined experimental and theoretical study of the metastable states of the Si^- ion. The experiments were performed at the Cryogenic Storage Ring (CSR) [21] at the Max Planck Institute for Nuclear Physics in Heidelberg.

The Si^- anion has three electrons in the same, half-filled $3p$ orbital. The configuration gives rise to a ^4S ground state with an electron affinity (EA) near 1.39 eV [22–24], and two doublet terms ^2D and ^2P; a level diagram is shown in Fig. 1. A significant metastable population in the ^2D term was observed in photodetachment measurements with a Si^- beam as early as 1971 [23]. Laser photoelectron spectrometry [24] resulted in binding energies (with respect to the neutral Si ground state) of (1.385 ± 0.005) eV for ^4S and (0.523 ± 0.003) eV for ^2D. This experiment, using a Si^- beam, also revealed a small but well-observable population of the ^2P term at a binding energy of (0.029 ± 0.005) eV. Later measurements [25] by infrared (IR) laser spectroscopy improved the accuracy of the EA and also yielded the individual ^2D binding energies of $(0.527\,234 \pm 0.000\,025)$ and $(0.525\,480 \pm 0.000\,020)$ eV for the $J = 3/2$ and $J = 5/2$ levels, respectively, indicating a fine-structure splitting of $(1.746 \pm 0.025) \times 10^{-3}$ eV. The ^2P fine-structure splitting was estimated [24] to be $\sim 1.6 \times 10^{-3}$ eV from isoelectronic extrapolation. The most accurate determination of the EA of Si was achieved by photodetachment microscopy [26,27], with the most recent measurement resulting in $(1.389\,521\,0 \pm 0.000\,000\,7)$ eV [28].

TABLE I. Theoretical radiative lifetimes for the metastable states of Si^-, calculated using the MCDHF method (present work) together with previous values given in O'Malley and Beck [29] and Andersson *et al.* [16].

State	O'Malley-Beck (2003)	Andersson *et al.* (2006)	Present work
$^2P_{3/2}$		25.1 s	(20.6±1.6) s
$^2P_{1/2}$	23.6 s	28.1 s	(22.1±1.5) s
$^2D_{5/2}$	27.3 h	12.2 h	(9.6±0.7) h
$^2D_{3/2}$	162 s	14.5 h	(11.9±0.8) h

The levels in the ^2D term appeared stable on the timescale of the first beam experiments. Their decay is forbidden by the parity selection rule and requires spin unpairing for two of the electrons to form the ^4S ground state. Hence, transitions become possible by relativistic effects only. In previous work, predictions for the lifetimes of the states with $J = 3/2$ and $J = 5/2$ in the ^2D term differ substantially between each other and are subject to unresolved controversy. In relativistic configuration interaction calculations, O'Malley and Beck [29] obtained a lifetime of 27.3 h for states with $J = 5/2$ symmetry in the ^2D term. However, for the $J = 3/2$ level, they predict that mixing with states of the same J in other terms and configurations reduces the lifetime to 162 s. Later multiconfiguration Dirac-Hartree-Fock (MCDHF) calculations of Ref. [16] found a different behavior, where the ^2D lifetimes are between 12 and 15 h for both J (see Table I). Both studies emphasize the high sensitivity of these transition rates to small admixtures in the atomic wave functions from relativistic configuration interactions.

Previous storage ring experiments on negative ions [16] included measurements on Si^- and studied the temporal behavior of the photodetachment signal selectively for states bound by less than 1.17 eV, thus excluding the ^4S ground state. The limited storage time allowed this experiment to derive only a lower limit of >60 s for the ^2D lifetime, which does not resolve the controversy.

The lifetimes of the ^2P levels were predicted to be in the range of 23–29 s [16,29]. The ^2P levels could not be observed in the previous storage ring experiments [16]. The authors attributed the observed photodetachment signal to the ^2D states exclusively, considering the ^2P states to be too weakly bound to survive the harsh conditions in the ion source and the black-body radiation field inside the storage ring.

The present work improves the situation in several respects. Experimentally, we observe the metastable decay under much more controlled conditions, in an extremely high vacuum and at low temperature. This allows for much longer storage times and reduces the effects caused by the ambient radiation field. Furthermore, we have carried out updated MCDHF calculations with a systematic, large-scale expansion of the space of configuration functions used. Our calculations compare favorably with recent experimental results on level energies and fine-structure splittings.

This paper is organized as follows: Section II describes theoretical calculations of radiative lifetimes and photodetachment cross sections. Section III provides an outline of the experimental setup. In Sec. IV, we present the storage ring experiments. We have found that in the long lifetime regime that we explore here, it is crucial to avoid misinterpretation of the data and carefully rule out possible instrumental effects on the observed decay constants. Therefore, we begin the experimental section with an overview of the decay of the metastable state signal compared with the overall beam decay in the storage ring, followed by laser depletion measurements and coincidence measurements with a pulsed laser. This stepwise analysis allows us to unambiguously identify an average natural lifetime for the weakly bound and sparsely populated ^2P states, and a lower lifetime limit for the long-lived ^2D states, both of which go considerably beyond the findings of previous experimental studies. Section V gives a summary and conclusions.

II. THEORY

A. Radiative lifetimes

We have used the MCDHF method [30], in combination with the relativistic configuration interaction (RCI) approach, to independently predict the electron affinities, fine-structure splittings, transition energies, and radiative lifetimes of the bound states of the negative Si^- ion. Within the MCDHF scheme, the wave function of each of these many-electron atomic states, also called atomic state function (ASF), is given as a linear combination of configuration state functions (CSFs) with common total angular momentum (J), magnetic (M), and parity (P) quantum numbers: $|\Gamma PJM\rangle = \sum_k c_k|\gamma_k PJM\rangle$. The CSFs $|\gamma_k PJM\rangle$ are constructed as jj-coupled Slater determinants of one-electron orbitals, and γ_k summarizes all the information needed to fully define the CSF, i.e., the orbital occupation and coupling of single-electron angular momenta. Γ collectively denotes all the γ_k included in the representation of the corresponding ASF. After solving the self-consistent MCDHF equations for the radial orbitals and the mixing coefficients c_k, corrections arising from the Breit interaction and approximate quantum electrodynamic terms are accounted for in the RCI calculations. The latter are found to be negligible for the valence electrons of such a light anion.

Since the outermost electron is weakly bound to the atom, correlation effects dominantly determine the structure of the anions [31]. Therefore, the ASFs have to be expanded in a large CSF basis to accurately account for correlation contributions. For Si^-, two schemes are employed in our calculations. In the first scheme, the set of the CSFs is generated by single and double (SD) excitations of electrons from the $3s^23p^3$ valence orbitals to high-lying virtual orbitals, with the most relevant triple and quadruple excitations being included via SD excitations from the $\{3s^23p^3,\ 3s3p^33d,\ 3s^23p3d^2,\ 3p^33d^2,\ 3s3p^34s,\ 3s^23p4s^2,\ 3s^23p^24p,\ 3s^23p4p^2,\ 3s3p^34d,\ 3s^23p4d^2\}$ multireference configurations. The convergence of the binding energies and lifetimes is monitored via layer-by-layer expansion and optimization of the active space of virtual orbitals from the $3d$ up to the $10l$ subshell. With 3 478 527 CSFs being generated for total angular momentum $1/2 \leqslant J \leqslant 5/2$, the calculated excited energies of the ^2D and ^2P states deviate by 1.8% with respect to the experimental values [24,25]. In the second scheme, the full triple excitations from the $3s^23p^3$ configuration up to $9l$ and the full quadruple excitations from the aforementioned multireference configurations up to $5f$ are included in the first scheme. This scheme generates a 7 327 283 CSF basis set, which effectively accounts for the most important quintuple excitations. As a result, the calculated excited state energies of 0.869 17 and 0.870 88 eV for the $^2D_{3/2}$ and $^2D_{5/2}$ states, respectively, and 1.369 03 and 1.372 90 eV for the $^2P_{1/2}$ and $^2P_{3/2}$ states, respectively, only differ by 0.9% with respect to the experimental values [24,25]. Though the 3.87 meV fine-structure splitting between the two ^2P states has not been measured yet, our calculated 1.71 meV fine-structure splitting for the ^2D term is close to the experimental (1.746 ± 0.025) meV splitting obtained from earlier laser photodetachment spectroscopy [25]. Furthermore, the first MCDHF-RCI scheme is also employed to calculate the binding energies of the $[\mathrm{Ne}]3s^23p^2\ ^3P_{0,1,2}$, $^1D_2$, and $^1S_0$ states of the neutral Si atom. With a total of 602 646 CSFs for $0 \leqslant J \leqslant 4$ being generated from the $\{3s^23p^2,\ 3s^23p^2,\ 3s3p^23d,\ 3s^23d^2,\ 3p^23d^2,\ 3s3p^24s,\ 3p^24s^2,\ 3s^24p^2,\ 3s^23p4p,\ 3s3p^24d,\ 3s^24d^2\}$ multireference configurations, we derive a theoretical electron affinity (EA) of 1.395 eV for the $^4S_{3/2}$ ground state of Si^-, which agrees to within 0.4% with the $(1.389\,521\,0 \pm 0.000\,000\,7)$ eV experimental EA [28].

Both the ^2D and ^2P states decay radiatively through magnetic dipole $M1$ and electric quadrupole $E2$ transitions, and thus they are metastable. Based on the second MCDHF-RCI scheme, the calculated radiative lifetimes of these Si^- states are shown in Table I. They are (11.9 ± 0.8) and (9.6 ± 0.7) h for the $^2D_{3/2}$ and $^2D_{5/2}$ states, respectively, and (22.1 ± 1.5) and (20.6 ± 1.6) s for the $^2P_{1/2}$ and $^2P_{3/2}$ states, respectively. The uncertainties are derived from the largest difference with respect to the lifetimes obtained from the first scheme. We find that our lifetime results are somewhat shorter than previous MCDHF predictions [16], due to the inclusion of more relevant CSFs in our calculations.

B. Photodetachment cross sections

To support the analysis of the experimental data, we have carried out dedicated calculations of the photodetachment cross section of all anionic states of Si^- at two specific photon energies, corresponding to wavelengths of 1390 and 635 nm. The choice of the photon energies is motivated by our lifetime measurements, which will be described in Sec. IV A.

As in the calculations outlined above, all atomic state functions for the description of the neutral atoms as well as the negatively charged Si ions have been generated by means of the MCDHF method. Here, we use the GRASP2K [32] and RATIP codes [33] to evaluate all the required transition amplitudes for modeling the photodetachment paths. While the discussion below is based mainly on a single-configuration notation, configuration mixing has been taken into account in the representation of the atomic states.

The photodetachment of an initial state $|\psi_i(P_iJ_i)\rangle$ with $N+1$ electrons into a final bound state $|\psi_f(P_fJ_f)\rangle$ of the

TABLE II. Calculated photodetachment cross sections σ_{pd} for all anionic states of Si^- at two laser wavelengths of 1390 and 635 nm, in units of megabarn (10^{-18} cm^2).

Transition	σ_{pd}(1390 nm)	σ_{pd}(635 nm)
$^4S_{3/2} \rightarrow {}^3P_0$		0.79
$\rightarrow {}^3P_1$		1.93
$\rightarrow {}^3P_2$		2.71
$^2D_{3/2} \rightarrow {}^3P_0$	1.26	1.09
$\rightarrow {}^3P_1$	3.38	2.34
$\rightarrow {}^3P_2$	0.40	0.49
$\rightarrow {}^1D_2$		3.19
$^2D_{5/2} \rightarrow {}^3P_0$	1.1×10^{-5}	1.2×10^{-4}
$\rightarrow {}^3P_1$	0.26	0.54
$\rightarrow {}^3P_2$	2.64	2.27
$\rightarrow {}^1D_2$		1.69
$^2P_{1/2} \rightarrow {}^3P_0$	0.79	1.45
$\rightarrow {}^3P_1$	3.31	3.67
$\rightarrow {}^3P_2$	2.34	2.79
$\rightarrow {}^1D_2$	3.15	4.66
$\rightarrow {}^1S_0$		4.06
$^2P_{3/2} \rightarrow {}^3P_0$	0.12	0.27
$\rightarrow {}^3P_1$	0.69	1.12
$\rightarrow {}^3P_2$	2.60	3.45
$\rightarrow {}^1D_2$	1.19	2.59
$\rightarrow {}^1S_0$		3.10

N-electron photodetached ion requires a photon energy $\hbar\omega > E_i(N+1) - E_f(N)$. The photodetachment amplitudes for this process into some final scattering state $|\psi_t\rangle = |\psi(P_t J_t M_t)\rangle$ (including the continuum electron) are given by

$$M^{(\pi L)}_{J_i \rightarrow J_f l j J_t} \equiv \langle (\psi_f, \epsilon\kappa) P_t J_t || H_\gamma(\pi L) || \psi_i(P_i J_i) \rangle, \qquad (1)$$

where $H_\gamma(\pi L)$ refers to the electron-photon coupling operator for multipole fields of parity π and angular momentum L (details can be obtained, e.g., from [33]). Boundary conditions are applied on the partial waves of the outgoing photoelectron with kinetic energy ϵ and relativistic angular momentum quantum number κ [$\kappa = \pm(j + 1/2)$ for $l = j \pm 1/2$] by including proper phases [34].

The photodetachment cross section for various final states $|\psi_f(P_f J_f)\rangle$ is given as

$$\sigma(P_f J_f) = \frac{4\pi^2 \alpha \omega}{3(2J_i + 1)} \sum_{\kappa, J_t} \sum_{\pi, L} \left| M^{(\pi L)}_{J_i \rightarrow J_f l j J_t} \right|^2. \qquad (2)$$

The summation in the above equation is performed over all possible partial waves of the photoelectron with kinetic energy $\epsilon = E_i + \hbar\omega - E_f$ as well as over the allowed continuum states $|\psi_t\rangle$. Here, α stands for the fine-structure constant. Table II shows the calculated photodetachment cross sections for Si^- at the relevant experimental photon energies of 0.89 and 1.95 eV. Using the reduced matrix elements in the above equation effectively implies an average over the initial magnetic substates of the system and a summation over the final ones.

The calculated cross section is used to estimate the depletion timescale of the metastable ^2D states in Sec. IV A. It is also observed that the excited state photodetachment cross sections are not larger in magnitude compared to the ground-state photodetachment cross sections. This observation will be used in Sec. IV A 2 to determine the lifetime limit. The calculated values have an uncertainty of about 40%, estimated from the gauge invariance of the results. We have included higher orbital angular quantum numbers (up to the g wave wherever possible) in the description of the detached electron; however, the main contributions are from s and d waves (in a few channels). The g wave does not have a significant contribution. In the case of photodetachment in the $^2D_{5/2}$ to $^3P_0$ channel, the cross sections are very small because the s wave contribution, which is dominant in most of the channels, is not present. In this case, the d wave is the main contributor. The cross sections in the $^2P_{1/2}$ and $^2P_{3/2}$ to $^1S_0$ channels are unusually high, which could be due to the inclusion of d and g waves in the calculations. For the infrared laser (1390 nm), the cross sections in a few channels are missing because they are energetically forbidden.

Although very little literature is available on photodetachment from Si^-, we have compared the present total photodetachment cross section at 1.95 eV to the theoretical data of Robinson and Geltman [37] and Gribakin and collaborators [38]. The present cross section is 44.2 Mb, whereas the values presented by Robinson and Geltman [37] and Gribakin *et al.* [38] are 27.0 and 47.0 Mb, respectively. Given the assessed uncertainty of our calculations, we find that our cross sections compare reasonably well with these data. Although our calculations are not extremely accurate, the compliance with these theoretical values gives confidence in their reliability.

III. EXPERIMENTAL SETUP

The measurements made use of the capabilities of the Cryogenic Storage Ring (CSR) [21] at the Max Planck Institute for Nuclear Physics. The CSR is a fully electrostatic storage ring with a circumference of 35 m. It features a nested vacuum structure with an outer cryostat and inner ultrahigh vacuum chambers that are cooled to 5 K by a liquid helium circuit. The stored ions are held on the revolving orbit by families of parallel deflectors and quadrupoles, which are all located inside the inner vacuum chambers. Detailed information on the storage ring parameters and performance can be found in [21]. Efficient cooling of internal degrees of positive [39] as well as negative [40] molecular ions by spontaneous emission of radiation has been demonstrated inside the CSR, and measurements using the electron cooler have been recently published [41].

For all measurements described here, the $^{28}Si^-$ ions were produced in a sputter ion source, mass selected by a dipole magnet, and accelerated to ~58 keV, prior to injection into the storage ring. The number of stored ions can be determined by a capacitive pickup electrode. For the present data sets, the number of initially stored ions was usually between 1×10^7 and 1×10^9.

To photodetach the outer electron, we used various continuous wave (cw) lasers and a pulsed optical parametric oscillator (OPO) that were coupled into the storage ring at different entry viewports. Figure 2 shows the straight section of the CSR that is used for laser experiments, together with

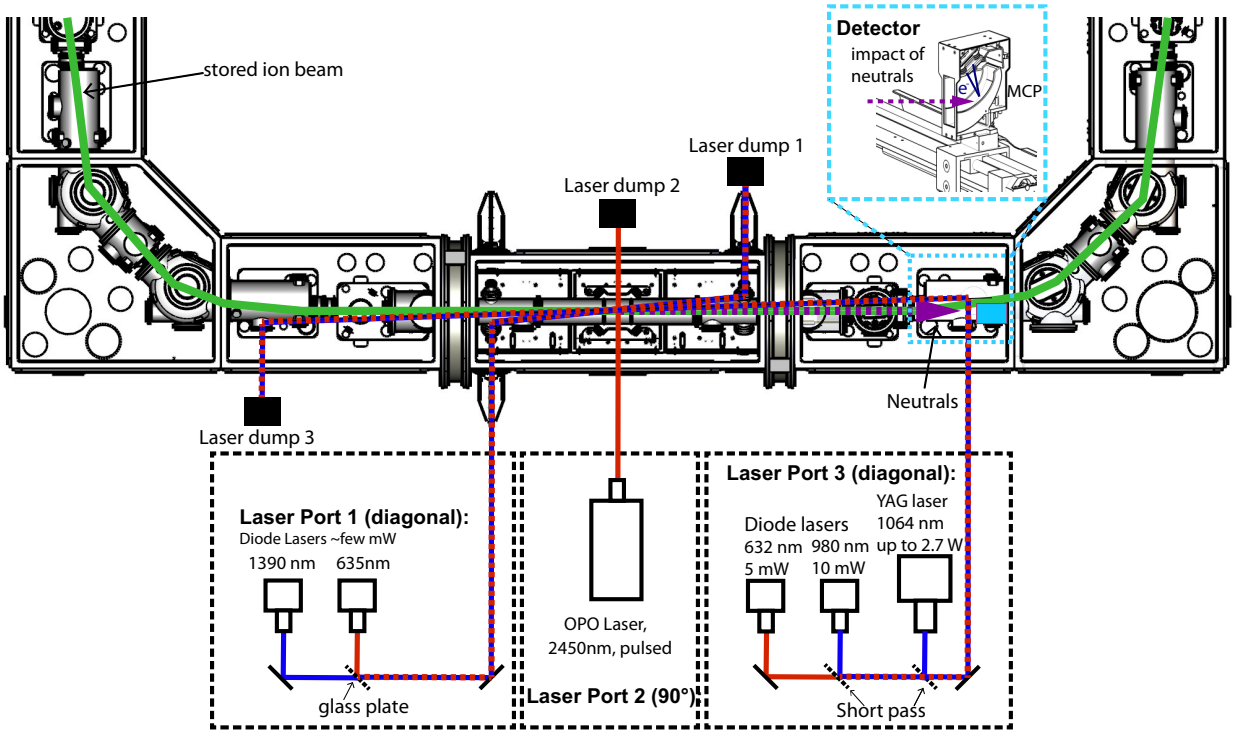

FIG. 2. Schematic of the laser interaction section at the CSR and the experimental setup (not to scale). The insets show simplified sketches of the optical setups (for the sake of simplicity, not all mirrors and optical elements are shown) at the laser entry ports, and the movable single-particle detector (cold movable particle counter, COMPACT [35,36]) that was used to detect the neutralized atoms in the present experiment.

a very simplified sketch of the laser setups and the particle detector used to record the neutralization events. Not shown is the electron cooler setup, which was introduced after the first set of measurements (described in Sec. IV A), but not used for any of the measurements reported here. The first and third laser ports allow for a diagonal laser-ion beam overlap, at grazing angles of 3.4° and 1.1°, respectively. Laser port 1 was used for the experiments before the installation of the electron cooler, and laser port 3 was used for experiments after the installation (described in Secs. IV B and IV C), as the laser access to the CSR had to be altered for the upgrade. The beam path for the diagonal entry ports is more complicated in reality than can be shown in a simple two-dimensional sketch, and the lasers are situated on an optical table at the base of the CSR support. The laser beam has to pass through several viewports and cryogenic shield layers to enter the experimental vacuum. Two of the laser mirrors are placed permanently inside the CSR experimental vacuum. These mirrors have a dielectric broadband coating suitable for wavelengths between 300 and 2000 nm. To couple in longer wavelengths, laser port 2 with a simple 90° crossed beams arrangement has to be used. The small intersecting angle of the diagonal laser path results in a more efficient overlap between the ion beam and the laser, and therefore it permitted us to work with lower laser power levels. Consequently, a grazing laser path was chosen whenever possible.

In all cases, the laser beams were shaped by telescopes outside the ring and were not focused in the interaction region. Within the CSR, the laser beam diameter was at least of the order of 5 mm (>0.2 cm^2 cross section). For all the continuous probing lasers described below, this yields intensity levels of <0.1 W/cm^2, while for the pulsed OPO laser described in Sec. IV C, the peak intensity was well below 10^4 W/cm^2 (at 2450 nm). Even this last intensity was still a factor of 10^3 lower than the intensity at which two-photon processes were quoted to be strongly suppressed in the previous study of Si^- by Scheer *et al.* [25]. From the result of Fig. 11 of Ref. [25], showing near-threshold two-photon detachment of ground state Si^- at 10^{10} W/cm^2, we estimate the level of two-photon detachment even at our pulsed power to be suppressed by a factor of $\sim 10^{12}$. Hence, at the applied laser power levels, we neglect multiphoton processes in our considerations.

The neutral Si atoms resulting from photodetachment were detected by a movable single-particle detector [35,36] that is situated downstream of the first 6°-deflector following the laser interaction section.

IV. EXPERIMENT

A. Low-background measurements

Two continuous wave lasers were utilized to neutralize the stored ions: a 635 nm (1.95 eV) visible (Vis) laser that is able to detach all states of the Si^- ion, including the ground state, and a 1390 nm (0.89 eV) infrared (IR) laser, which selectively detaches only the excited ^2D and ^2P states (see Fig. 1). With a time structure described below, neutral Si atoms were counted on the downstream detector with overlapped laser beams as well as in their absence. The IR laser had a power of 18 mW that was somewhat reduced during the passage through a thin glass plate that was used to merge the two beams outside the

CSR. About ∼15 mW were sent into the CSR and superimposed to the ion beam at a grazing angle of 3.4° (see Fig. 2). However, as the present data were taken at the end of a cold period that lasted for several months, the laser windows inside the cryostat had accumulated a thin icy layer (in the meantime, we have modified all viewports to prevent this effect). Because the beam had to pass several viewports, the intensity at the exit port was reduced to less than a percent of the initial power that was sent in. Consequently, the power that the ion beam has been exposed to was also only a small fraction of the initial laser power. We estimate an effective power level of no more than ∼1 mW from the IR laser.

Since we expected most of the ions to be in the negative ground state, the Vis laser was chosen to be considerably weaker (4 mW) to avoid saturation of the detector. In this case, the power was further reduced because we injected only the reflection off the merging glass plate, and only about ∼0.5 mW were sent toward the CSR. The visible radiation was attenuated even more than the infrared radiation by the ice on the viewports, and at the exit port the beam was diluted so much that the power level could not be precisely determined. Since we are not interested in measuring absolute photodetachment cross sections (and, in any case, we do not know the precise spatial overlap between the ions and the laser beams), the beam attenuation is not a major concern. In fact, the low effective power levels that made it into the storage ring lead to a very long timescale for laser depletion of the metastables by photodetachment, which we will estimate in the following paragraph.

Both lasers were switched on and off by mechanical shutters during storage. One full cycle was 4 s long and consisted of the following pattern: [1 s: IR – 1 s: lasers off – 1 s: Vis – 1 s: lasers off]. This results in a duty cycle of $D = 1:4$ for both lasers. We will use the calculated photodetachment cross sections (Table II) to estimate the depletion timescale for the IR laser, as the Vis laser is much weaker and therefore depletion will be much slower. The characteristic timescale T_{pd} for laser depletion by photodetachment of the metastable states through the IR laser can be calculated as

$$T_{\mathrm{pd}}^{-1} = \sigma_{\mathrm{pd}} \Phi \frac{L_{\mathrm{ov}}}{L_{\mathrm{CSR}}} D, \tag{3}$$

where $\Phi = 8.9 \times 10^{15}\,\mathrm{cm}^{-2}\,\mathrm{s}^{-1}$ denotes the photon flux per second and area (assuming a laser radius of $r_{\mathrm{L}} = 0.5\,\mathrm{cm}$ and an effective laser power of 1 mW at a photon energy of 0.89 eV), while L_{ov} denotes the laser-ion overlap length, which at a grazing angle of $\theta = 3.4°$ corresponds to $L_{\mathrm{ov}} = 2r_{\mathrm{L}}/\sin\theta = 16.9\,\mathrm{cm}$, and which has to be divided by the length of the storage ring closed orbit $L_{\mathrm{CSR}} = 3500\,\mathrm{cm}$. Considering the photodetachment cross sections for the metastable states, we are mainly interested in the effect on the long-lived ^2D states, as photodetachment at the present power levels is much too slow to have an impact on the short-lived ^2P states. We sum up the calculated values of the cross sections to the various neutral states (Table II), resulting in $\sigma_{\mathrm{pd}} = 5.04 \times 10^{-18}\,\mathrm{cm}^2$ for the $^2D_{3/2}$ state and $\sigma_{\mathrm{pd}} = 2.90 \times 10^{-18}\,\mathrm{cm}^2$ for the $^2D_{5/2}$ state. These values are weighted with the multiplicities of the two states to derive an effective cross section of $\sigma_{\mathrm{pd}}^{\mathrm{eff}} = 3.76 \times 10^{-18}\,\mathrm{cm}^2$. With these numbers, the characteristic depletion timescale is $T_{\mathrm{pd}} = 2.5 \times 10^4$ s. We note that this number is only a coarse estimate since we do not know the exact laser power inside the ring and since the laser path had not been tuned for optimal overlap. Furthermore, the calculated cross sections are assumed to have an uncertainty of 40%. Nevertheless, this long depletion timescale is of relevance in later sections, where we embark on a comparison of the photodetachment signals for both lasers at long storage times.

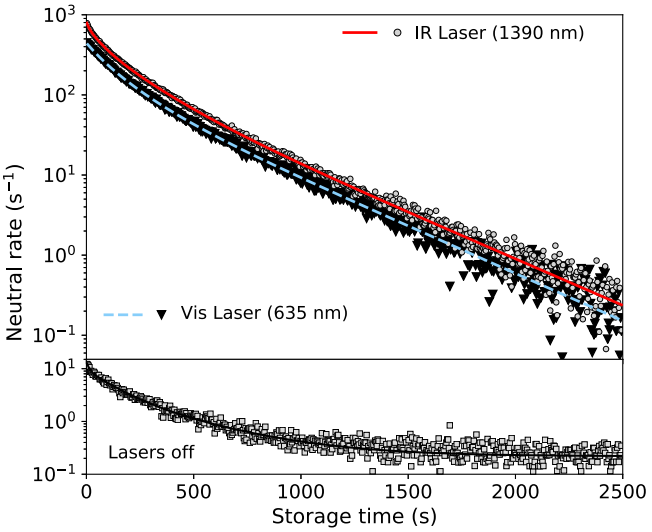

FIG. 3. Photodetachment signals from both continuous lasers plotted as a function of the storage time (upper panel). The solid line depicts a four-exponential fit to the signal from the IR laser (gray dots), the dashed line shows a three-exponential fit to the signal from the Vis laser (black triangles). The lower panel shows the background rate measured during the laser-off phases (gray squares). Fit parameters are given in Table III.

To analyze the data, the total counts and measurement time for each storage time bin were summed up for all injections and used to create plots of the count rate versus storage time, with a time bin width of 4 s, using combined statistical uncertainties. Error bars—when shown—represent the standard deviation σ of the count rates, found from the square root of the accumulated counts at the respective time bin, thus assuming Poisson counting statistics. A higher time resolution is not available if the bin width is to be a multiple of the full cycle pattern. No attempts at arbitrarily rebinning the data were made.

Figure 3 shows the photodetachment rates for both lasers (upper panel) and the count rate during the laser-off phases (lower panel). The data shown here represent 18 consecutive injections with a total data taking time of 13 h.

We expect the neutral rate during the laser-off phases to be dominated by two contributions: (1) a neutral signal caused by the collisional detachment of ions in the storage ring, and (2) a constant detector noise level which is reached after about 2000 s of storage. The background rate right after injection corresponds to 13 s^{-1}, which is much lower than both of the photodetachment signals. Following the reasoning outlined in [21], we can use this value together with the number of stored ions, $N_{\mathrm{ion}} = 2.9^{+0.4}_{-1.7} \times 10^8$ (for details on CSR diagnostics and uncertainties, see [21]), and a literature value for the absolute

TABLE III. Parameters for multiexponential fits shown in Fig. 3. The number of injected ions was $N_{\rm ion} = 2.9 \times 10^8$.

	τ_1 (s)	A_1 (s^{-1})	τ_2 (s)	A_2 (s^{-1})	τ_3 (s)	A_3 (s^{-1})	τ_4 (s)	A_4 (s^{-1})
Lasers off	351 ± 30	3.4 ± 0.7	123 ± 17	5.8 ± 0.5	14.0 ± 4.6	3.8 ± 0.7		
Vis laser	367.2 ± 5.0	137.1 ± 7.4	150 ± 12	221 ± 27	64 ± 13	87 ± 31		
IR laser	375.1 ± 5.5	185 ± 12	172 ± 10	318 ± 18	58.8 ± 8.0	218 ± 18	11.0 ± 3.0	96 ± 17

collisional detachment cross section, $\sigma_{\rm cd} = 7.7 \times 10^{-16}\,{\rm cm}^2$ [42], of Si^- ions in helium gas at the relevant energy (while detachment cross sections are known to vary slightly between He and H_2 target gas [43], we consider this value a reasonable estimate), to derive a coarse estimate for the residual gas density inside the storage ring of $n_{\rm rg} = 120^{+350}_{-80}\ {\rm cm}^{-3}$, compatible with the previous upper limit [21].

From the estimate of the particle density, the mean free path $\lambda = 1/(n_{\rm rg}\sigma_{\rm cd})$ can be calculated. The characteristic lifetime for collisional detachment is then given by $\tau_{\rm coll} = \lambda/v = 1.7 \times 10^5$ s, with v being the velocity of the Si^- ions. With this value being so large, we conclude that collisional detachment has no significant impact on the observed lifetimes for the low-background measurements shown here.

We can fit the background data by the sum of three exponential functions and a constant offset,

$$R(t) = \sum_{i=1}^{3} A_i \exp(-t/\tau_i) + c_0 \qquad (4)$$

(two or four exponentials are used in the same formula for other cases below). Here the value for $c_0 = (0.219 \pm 0.007)\,{\rm s}^{-1}$ can be attributed to the constant detector noise; the amplitudes and lifetimes for the exponential fit function are given in the first row of Table III. In the following, the background measured in the time bin directly after a laser-on step was subtracted from the count rates with laser beams to yield the photodetachment signals.

Comparing the photodetachment rates for both lasers, we find that the rate for the IR laser, although it photodetaches the *excited* Si^- levels only, essentially follows the course of the Vis laser signal, which includes photodetachment from the ground state. Although the IR intensity inside the ring is probably a factor of 50–100 higher than for the Vis laser, the IR/Vis rate ratio is only ∼1.5. Taking into account that the calculated cross sections are somewhat higher for photodetachment of the ^4S ground state with the Vis laser, when compared to photodetachment of the ^2D states with the IR laser, the ratio of the count rates suggests that the population of metastable states lies in the percent range (this result will be corroborated by depletion measurements shown in Sec. IV B 2).

We can achieve fair fits to the data using the sum of four exponentials (without any offset, as the background has already been subtracted) for the IR laser, while the fit to the Vis laser does not improve when more than three exponential functions are used. The fit parameters are given in Table III.

Regarding the temporal evolution, the only significant difference between the two signals shows up at short storage times, where the IR laser shows a steeper decay, corresponding to a lifetime around ∼11 s. The other three decay components with lifetimes around 60, 150–170, and 370 s are—within the error margins—identical for both lasers and are likely to represent beam-intensity decay, as discussed in the next section.

1. Dependence of the photodetachment signal on the number of stored ions

While the measurements shown in the previous section correspond, on average, to an injected ion number $N_{\rm ion} = 2.9 \times 10^8$, we also studied the effect of reducing and increasing this number by about a factor of 3. The results are shown in Fig. 4. We have modified the current of the ion beam in the transfer beam line to the CSR by closing a variable aperture, in order to change the number of injected ions without changing the ion source conditions. This procedure may also change the beam emittance, but in our experience this has a minor effect on the initial storage conditions, as the CSR acceptance is much larger than the maximum emittance allowed by the geometry of the transfer beam line.

The signals, observed with the Vis laser and thus representing all anionic Si^- states, show considerable differences at short storage times, with higher numbers of injected ions leading to a steeper initial decay. We have fitted the curves with sums of two or three exponential functions. The fit parameters are given in Table IV. The amplitudes for the respective exponential functions have been normalized to unity and denoted by A_i^N to facilitate comparisons of the relative strengths of the different lifetime components among the runs.

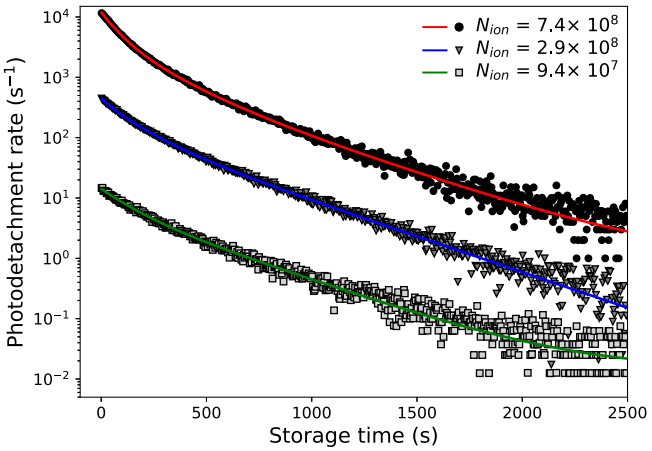

FIG. 4. Photodetachment signals obtained using the Vis laser for three runs with different average numbers of injected ions. For clarity, the uppermost and lowermost curves have both been shifted by an order of magnitude, by multiplying them with factors of 10 and 0.1, respectively. The solid lines depict fits to the data. The fit parameters are given in Table IV.

TABLE IV. Fit parameters for measurements with different numbers of injected ions, N_{ion}.

N_{ion}	τ_1 (s)	$A_1^N(\text{s}^{-1})$	τ_2 (s)	$A_2^N(\text{s}^{-1})$	τ_3 (s)	$A_3^N(\text{s}^{-1})$
7.4×10^8	380.6	0.11	175.7	0.33	69.6	0.57
2.9×10^8	367.2	0.30	149.9	0.50	64.0	0.20
9.4×10^7	367.9	0.46	128.9	0.54		

For the lowest number of ions, only two exponential functions were necessary for a good fit, while the higher N_{ion} required three exponentials. The amplitude of the short-lived component, with a lifetime around 60 s, strongly depends on the number of ions, and it is actually not distinguishable in the fit for the lowest N_{ion}. We attribute this lifetime to storage ring effects that increase with the number of injected ions. With a weaker dependence on N_{ion}, the two longer lifetime components remain, even as less ions are injected.

In previous experiments, diffusive momentum changes were observed for stored ions inside the CSR [21], on the timescale of the limiting storage times. This increase in the ion momentum is suspected to be the main cause of beam loss. Possible sources of diffusion could be noise of the storage fields, independent of the ion number, as well as effects related to ion-ion collisions or ion-beam space charge, which are expected to show an ion number dependence. The multiexponential decrease of the stored ion number, observed quite ubiquitously at the CSR, indicates a coexistence of such momentum diffusion effects.

We presently cannot give a detailed explanation of the physical processes behind the two beam-decay time constants τ_1 and τ_2 that remain at low injected ion numbers. In any case, the two exponential lifetime components suggest two independent loss mechanisms for the stored ions.

2. *Photodetachment signal at long storage times*

Apart from the difference at short storage times, the similarity of the time dependence of the photodetachment signals for both lasers is quite informative. The fact that the IR laser—which neutralizes only metastable ions–generates a signal at $t > 2000$ s indicates that there has to be at least one long-lived excited state, which is still present at that time. In order to get a lower limit of its lifetime, we can compare the decay constants of the photodetachment signals at long storage times (Fig. 5). At $t > 800$ s, a single-exponential function is sufficient to get an excellent fit for both signals. The resulting lifetimes of (360.1 ± 2.4) and (358.4 ± 3.0) s are identical within the error margins. Based on the signal size and the comparatively high IR intensity, it is plausible to assume that the photodetachment signal of the Vis laser is dominated by the negative ground state (we will describe corroborating results for this conjecture, in the form of laser depletion measurements, in the next section), and thus independent of changes in the state populations of the stored ion beam. Therefore, we can reason that its decay constant is representative of the intrinsic lifetime of the ions inside the CSR. This allows us to obtain a lower limit for the lifetime of the metastable state responsible for the IR laser signal at long storage times.

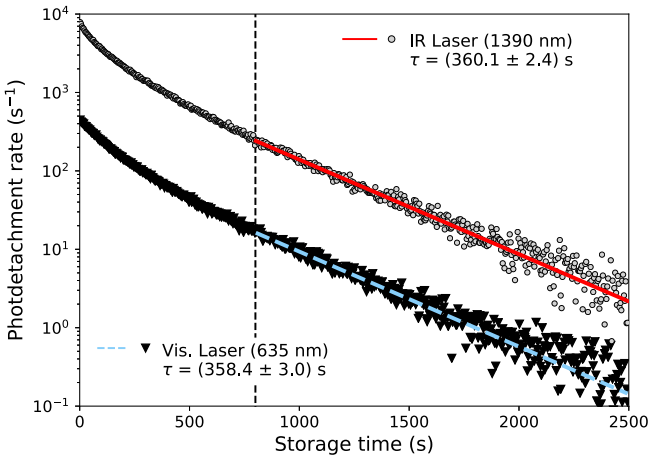

FIG. 5. Photodetachment signals for the IR laser (gray dots) and for the Vis laser (black triangles) fitted with a single exponential at storage times $t > 800$ s. For clarity, the IR laser signal has been multiplied by a factor of 10.

For simplicity, we assume that only two states remain populated, namely, the ground state (population N_g) and an excited state (population N_e) with a radiative decay constant k_r. The total number of ions that remains in the ring after 800 s is denoted by N, and the fraction of excited ions by η. The storage decay constant is denoted by k_{beam}. In this scenario, the population of the excited state will follow a simple exponential decay,

$$N_e(t) = \eta N \exp\left[-(k_r + k_{\text{beam}})t\right], \tag{5}$$

while the ground-state population can be described by

$$N_g(t) = N \exp(-k_{\text{beam}}\, t) - \eta N \exp[-(k_r + k_{\text{beam}})t]. \tag{6}$$

It is important to note that this simple set of equations is only valid if the beam lifetime, given by the storage ring properties and characterized by the decay constant k_{beam}, is identical for both the ground and excited states. We justify this assumption by pointing out that the collisional detachment rate is so small that it does not limit the storage time inside the CSR at all. As mentioned before, the experimental observations indicate that ion-beam dynamics, such as an increase in the momentum spread of the stored ions, are the cause for the limited beam lifetime [21]. The resulting beam loss rate is expected to be independent of the internal state of the stored ions.

The rate observed during laser exposure will be related to the respective populations by

$$\begin{aligned} R_{\text{IR}} &= f_e^{\text{IR}} N_e(t), \\ R_{\text{Vis}} &= f_g^{\text{Vis}} N_g(t) + f_e^{\text{Vis}} N_e(t), \end{aligned} \tag{7}$$

where f_e^{IR}, f_g^{Vis}, and f_e^{Vis} are constants that account for the laser interaction, including the geometric overlap between the lasers and the ion beam, their intensities in the interaction region, and the photodetachment cross section of the ground and excited states at the respective wavelength of the lasers. These model count rates can now be compared to the observed rates after 800 s of storage (Fig. 5). Considering the Vis laser first,

it is apparent that the measured rates are well represented by a single-exponential decay, while the model contains two decay constants. We reconcile this discrepancy by assuming that the majority of the ions after 800 s of storage populate the ground state, corresponding to $\eta \ll 1$. Based on our calculations of the photodetachment cross sections (Table II), we can also safely assume $\eta f_e^{\mathrm{Vis}} \ll f_g^{\mathrm{Vis}}$, i.e., the excited state does not have an extremely large photodetachment cross section at the frequency of the Vis laser, which could potentially dominate the photodetachment signal. The model rate of the Vis laser can then be reduced to

$$R_{\mathrm{Vis}} = f_g^{\mathrm{Vis}} N \exp(-k_{\mathrm{Vis}} t), \tag{8}$$

where, based on the assumptions $\eta \ll 1$ and $\eta f_e^{\mathrm{Vis}} \ll f_g^{\mathrm{Vis}}$, the decay constant of the Vis signal is $k_{\mathrm{Vis}} = k_{\mathrm{beam}}$. From its fitted decay time in Fig. 5, we find $\tau_{\mathrm{beam}} = 1/k_{\mathrm{beam}} = 1/k_{\mathrm{Vis}} = (358.4 \pm 3.0)$ s.

Even within our approximations, the rate of the excited state will still feature a different decay constant,

$$R_{\mathrm{IR}} = f_e^{\mathrm{IR}} \eta N \exp\left[-(k_r + k_{\mathrm{beam}})t\right]. \tag{9}$$

The decay constant of the IR signal is $k_{\mathrm{IR}} = k_r + k_{\mathrm{beam}}$. From its fitted decay time in Fig. 5, we find $1/(k_r + k_{\mathrm{beam}}) = 1/k_{\mathrm{IR}} = (360.1 \pm 2.4)$ s. In combination, we have

$$k_r = k_{\mathrm{IR}} - k_{\mathrm{Vis}} = (-1.32 \pm 2.98) \times 10^{-5}\ \mathrm{s}^{-1}. \tag{10}$$

The difference of the fitted decay constants is compatible with zero, indicating a very small value for k_r. Following the example of prominent experiments resulting in upper bounds [44,45], we choose to adopt a 90% confidence level (using the 1.645σ uncertainty of k_r only) to obtain the upper limit $k_r < 4.9 \times 10^{-5}\ \mathrm{s}^{-1}$. This results in a lower boundary for the metastable lifetime of

$$\tau_r > 2.0 \times 10^4\ \mathrm{s} = 5.7\ \mathrm{h}. \tag{11}$$

The present lifetime limit is of similar size as the evaluation of the depletion timescale of the metastable states through the IR laser, which we derived in Sec. IV A. The depletion timescale should, however, only be seen as a very coarse estimate, as the photodetachment cross sections and the effective laser power have large uncertainties. Based on the fact that the decay time constants of both photodetachment signals are identical within the error margins, we do not see any indication of laser depletion in the present data.

While our measurements do not permit us to derive a definite value for the lifetimes of the ^2D states, the long lifetime limit that we obtain from the comparison of the photodetachment signals highlights the potential of precise rate measurements with the very low background that cryogenic storage rings provide.

B. Laser depletion measurements

After the analysis of the initial data, we decided to undertake additional experiments to clarify open questions. Among the issues to be addressed were the the origin of the intermediate decay constants and the fraction of metastable ions in the beam.

1. Creation of a $^4S_{3/2}$ ground-state beam

To create a pure ground-state ($^4S_{3/2}$) anionic Si^- beam, we introduced a continuous laser with higher power to be able to deplete all the excited metastable ions. Such a depleted beam will not experience any internal state changes during storage. Any detachment signals (both laser and collision induced) are expected to reflect only the decay of the stored ion beam. We used a continuous wave Nd:YAG laser with a wavelength of 1064 nm and maximum power of 2.7 W at the diagonal laser port 3 (with a grazing angle of 1.1°), counterpropagating the ion beam (see, also, Fig. 2).

To probe the lifetime of the stored ions, we used two diode lasers aligned along the same path, one at a visible wavelength of 632 nm (1.95 eV) and one at an infrared wavelength of 980 nm (1.27 eV). Again, we denote these two lasers by Vis and IR, respectively, and, as before, the photon energy of the Vis laser allows for neutralization of all anionic states, while the IR laser will be able to neutralize only the metastable states. Both lasers had power levels of the order of a few mW. One full laser cycle extended over 10 s and the following pattern was employed: [0.5 s: IR – 4.5 s: lasers off – 0.5 s: Vis – 4.5 s: lasers off]. In addition, we introduced a depletion phase during the first 20 s of storage. In these initial 20 s, the full laser power of the Nd:YAG laser was used and we did not record data since the initial neutral flux would have saturated and potentially damaged the detector.

Figure 6 depicts the background-subtracted photodetachment signals for both probe lasers with and without the depletion phase. The panel on the lower right shows that in the depletion run, we did not observe any photodetachment signal from the IR probe laser, indicating that all ions in metastable states have been removed.

We fitted the signals with multicomponent exponentials, with the parameters given in Table V. A first comparison with the time constants observed in Sec. IV A (Table III) reveals a trend toward shorter storage times. This can be attributed to a much higher residual gas pressure inside the CSR, as the depletion measurements were carried out in an unbaked storage ring, after the installation of the electron target. In the photodetachment signals without the depletion laser, we also see very short-lived components around 10 s, which may be indicative of the presence of the ^2P states. This short-lived component is absent in the Vis laser signal after the depletion laser has been used, as the data taken in this case started after 20 s. The component around 60 s, which is present in the previous measurements with higher numbers of injected ions, is absent in all signals of Fig. 6 because we injected fewer ions.

The most important aspect of the measurements shown here is the fact that the lifetime $\tau_2 \sim 100$–120 s is the strongest component, with nearly unchanged strength relative to τ_1 in all the signals. The components with decay times τ_1 and τ_2 in the Vis laser signals remain at similar relative amplitudes (Table V) after all metastable states have been removed. This strongly suggests that the underlying decay is not caused by an internal state change of the stored ions, but has to be attributed to storage ring effects. Hence, we do not observe any signal requiring us to assume the decay of metastable ions with a lifetime of 162 s as predicted for the $^2D_{3/2}$ state in the calculations of O'Malley and Beck [29].

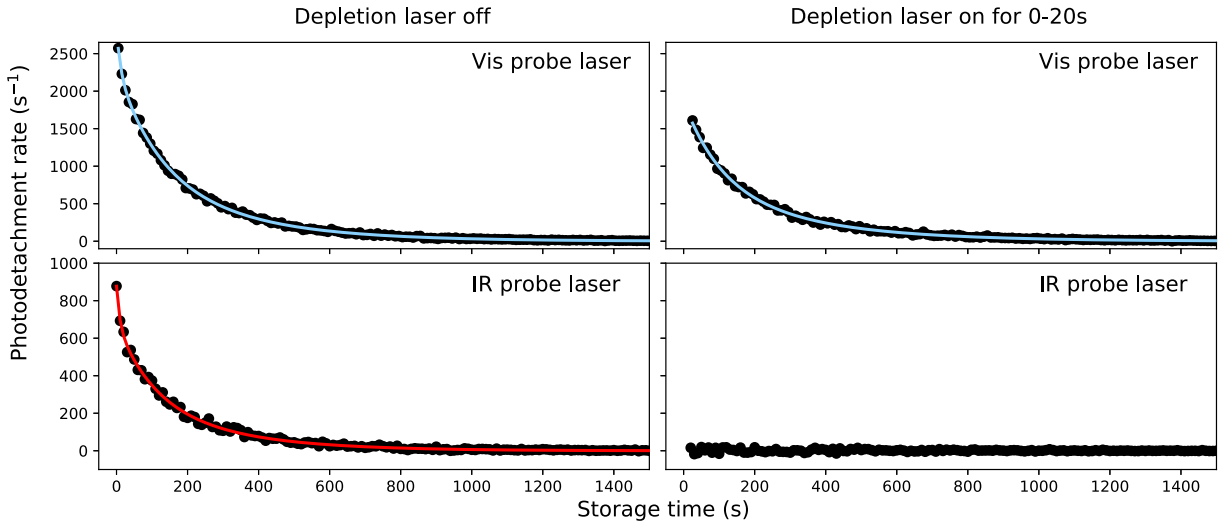

FIG. 6. Photodetachment signals from both probe lasers, measured with and without switching on the depletion laser for the first 20 s of storage (see labels). Laser-off background has been subtracted. The solid lines depict multiexponential fits (fit parameters are shown in Table V) to the photodetachment signals. The number of injected ions was $N_{\text{ion}} \sim 2.5 \times 10^7$ for both runs.

2. *Fraction of ions in metastable states*

We used the continuous Nd:YAG laser to quantify the total fraction of stored ions in metastable states. By reducing its output power to 30 mW, and at the same time adjusting the number of ions such that the detector stayed below saturation, we were able to follow and monitor the depletion for the first minute of storage. The neutralization signal caused by the Nd:YAG laser is shown in Fig. 7. Also visible is a step in the neutral signal after 60 s, when the laser is switched off and only the collisional detachment signal remains.

We injected a comparatively low number of 1×10^7 ions for this measurement, and we found that this leads to an almost single-exponential decay behavior in the neutral count rate during the first minute of storage (with the Nd:YAG laser switched off).

To estimate the number of metastable ions, we extrapolate the collisional detachment rate—seen after switching off the Nd:YAG laser—to shorter storage times and attribute all excess neutralization above that curve to photodetachment by the depletion laser. Assuming that photodetachment is the dominant loss process for metastable ions during the first minute of storage, we simply add all the neutral counts above the collisional detachment curve, which results in 30 000 neutrals coming from metastable ion photodetachment. Taking into account the detector efficiency $\epsilon = 0.09^{+0.12}_{-0.01}$ (while the detector itself has a rather high detection efficiency [35,36], the lower number used here is taking into account the finite detector size and thus geometric losses from the divergence of the uncooled beam [21]) and the initial number of stored ions, this results in a rough estimate of 3.3% for the fraction of all ions being in metastable states (within the above-mentioned assumptions and with an uncertainty of about a factor of 2.5). We made several similar measurements while changing the conditions in the ion source to see whether we could significantly increase this fraction, albeit without much success. Within our uncertainties, we did not notice any clear trend that we could correlate with the ion source conditions, and we were not able to achieve a significantly higher metastable fraction than the ∼3% reported above. This finding means that a sputter ion source may not be the best choice for experiments with metastable silicon anions. However, it also confirms once more that the metastable fraction is low enough to safely assume that the photodetachment signal of the Vis laser is dominated by the $^4S_{3/2}$ negative ground state, which we implied for the derivation of the lifetime limits of the ^2D states in Sec. IV A 2.

C. Decay of the ^2P states observed with a pulsed laser

We used a pulsed laser at longer wavelength to selectively probe the weakly bound ^2P states. Since collisional detachment rates during these measurements were higher than usual (owing to increased residual gas densities in an unbaked storage ring), we employed coincidence counting with nanosecond laser pulses for background suppression. We used an Ekspla NT342b OPO laser at 2450 nm (corresponding to 0.506 eV). This photon energy is just low enough to detach the ^2P states exclusively.

TABLE V. Parameters of the multiexponential fits to the photodetachment signals of Fig. 6.

	τ_1 (s)	A_1 (s^{-1})	τ_2 (s)	A_2 (s^{-1})	τ_3 (s)	A_3 (s^{-1})
Vis laser, no depletion	288 ± 13	1022 ± 125	116 ± 11	1282 ± 98	10.9 ± 4.4	533 ± 118
IR laser, no depletion	263 ± 21	308 ± 69	101 ± 20	374 ± 55	8.9 ± 4.7	196 ± 48
Vis laser, depletion	306.9 ± 6.8	813 ± 50	104.2 ± 7.1	1049 ± 46		

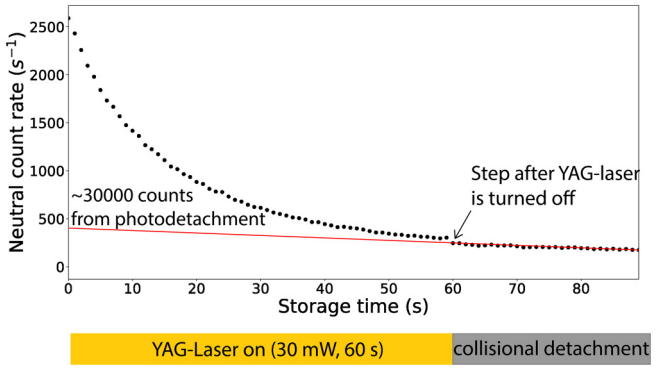

FIG. 7. Neutral count rates during a depletion run at comparatively low power. The Nd:YAG laser was switched on for 60 s. The red curve shows a single-exponential decay, which is fitted to the laser-off phase and extrapolated to shorter times. The number of counts from photodetachment is derived by integration of the events during the laser-on phase after subtraction of the extrapolated curve. We can use this value to estimate the fraction of ions in metastable states (see main text for details).

The laser had to be operated at the edge of its tuning range and the output was very low (of the order of 1 μJ per pulse). Furthermore, we could not use a diagonal laser path for these measurements, as the broadband mirrors inside the CSR experimental vacuum can only be used at wavelengths <2 μm. Therefore, we resorted to a crossed beam path through the middle of the straight storage ring section, at a 90° angle to the ion beam (see Fig. 2), significantly reducing the beam overlap. Nevertheless, the advantage of using a pulsed laser is a very strong suppression of continuous background counts, as the energy of one laser pulse is delivered within the short time interval of ~5 ns, with a repetition rate of 20 Hz.

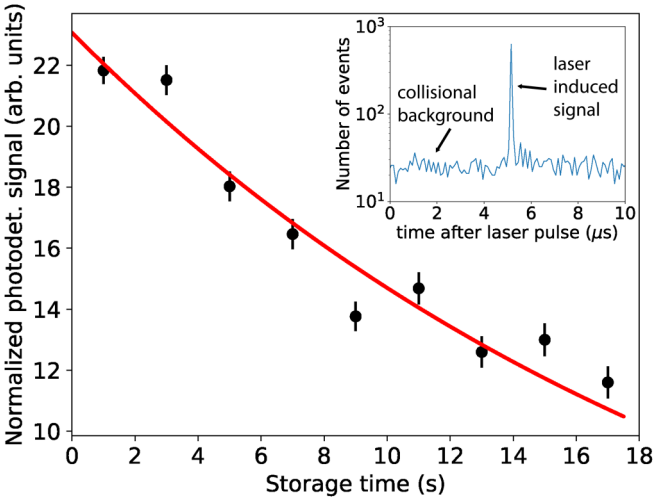

FIG. 8. Background-subtracted normalized photodetachment signal obtained using the pulsed OPO laser. The laser was operated at 2450 nm to exclusively photodetach the weakly bound ^2P states. The red line shows a single-exponential fit, yielding a lifetime $\tau = (22.2 \pm 2.5)$ s. Inset: Neutral counts as a function of time after the OPO laser pulse.

The inset of Fig. 8 shows the event counts as a function of time after the laser pulse, for a ~5 h measurement time (~3×10^5 laser pulses). We clearly observe a laser-induced signal at the expected time of flight after the laser shots. Owing to the crossed beams arrangement and the very low laser power, the signal is rather weak, but still easily distinguishable from the background. At up to 10^9 Si^- ions injected every 20 s, we typically observed less than one photodetachment event per injection.

To analyze the data, we defined a narrow time window around the laser-induced signal. We averaged the collisional background events outside of the time window and subtracted the average from the events inside, thus deriving the background-subtracted photodetachment signal. Furthermore, we used the recorded average of the collisional background as a function of storage time as a proxy for the decay of the number of ions in the ring. Dividing the photodetachment signal by the averaged collisional background in each storage time bin, we obtain a normalized photodetachment signal, whose decay is expected to be independent of ion-beam loss processes, plotted in Fig. 8. A single-exponential fit to the data results in a lifetime of $\tau = (22.2 \pm 2.5)$ s.

We assign the experimental result τ from Fig. 8 to the combined decay of the two ^2P states of Si^-. Comparing this value to the theoretical predictions (Table I), we find our experimental value to be in excellent agreement with the MCDHF calculations carried out for the present work and with the single value for the $^2P_{1/2}$ state given by O'Malley and Beck [29], while the values obtained by previous MCDHF calculations given in Andersson *et al.* [16] are somewhat larger.

V. SUMMARY AND CONCLUSION

The metastable states of the silicon anion, with its $3p^3$ (half-filled shell) electron configuration, represent an intriguing case for lifetime studies, which become challenging through the small predicted decay rates and binding energies for some of the levels. The low temperatures and extreme vacuum inside the CSR allowed us to observe the anionic states with minor external perturbations. By careful stepwise interpretation of the time dependencies in the photodetachment signals at different wavelengths, we were able to extract specific lifetime data on the metastable anionic states that were inaccessible to previous experiments.

Our measurements with pulsed midinfrared radiation give definitive proof that at least one short-lived and weakly bound metastable level was present in the stored ion beam, which can with high certainty be attributed to the ^2P term of Si^-. We find a lifetime of $\tau = (22.2 \pm 2.5)$ s by probing with 2.45 μm laser pulses that can only detach this weakly bound level. The measured radiative lifetime τ is in very good agreement with our updated MCDHF calculations and the lifetime calculated for the $^2P_{1/2}$ state by O'Malley and Beck [29], and slightly shorter than the lifetime values given for this term in Andersson *et al.*, which ranges from 25.1 to 28.1 s [16].

The laser depletion measurements indicate that the fraction of metastable (^2D and ^2P) Si^- ions produced in the sputter ion source is of the order of 3% (with a large uncertainty of a factor of 2.5). To increase the fraction of metastables states for future experiments, the process of double electron capture

by a positively charged Si^+ beam in a vapor cell could be considered, as demonstrated by Lee *et al.* [46] for C^- (^2D).

The similarity of the photodetachment signal from metastable Si^- levels at long storage time to that from all Si^- ions, together with depletion measurements probing the metastable fraction, demonstrate the existence of at least one very long-lived metastable anionic state, with a lifetime >5.7 h at 90% confidence level. Based on the theoretical calculations, it seems plausible to assign this long lifetime to a ^2D state. The predicted lifetime of 162 s for the $^2D_{3/2}$ fine-structure level in the calculations of O'Malley and Beck [29] is not supported by our data. While we do find intermediate lifetime components around $\sim$120 s in the observed decay signals, the persistence of these lifetime components in depletion measurements, removing all excited Si^- states, gives a strong indication that these lifetime components are caused by the storage ring, rather than metastable decay. One could argue that the $^2D_{3/2}$ fine-structure level in question may not be populated by our ion source, but that seems highly unlikely, as previous measurements found the populations in the two ^2D fine-structure levels to be close to thermal [25].

Hence, we find our results at longer storage times in better agreement with our present MCDHF calculations, as well as the previous calculations of Ref. [16] that give slightly longer values. While we cannot give a definitive lifetime value for the ^2D states, we can infer a lower limit of 5.7 h, which makes this, to the best of our knowledge, the longest lifetime limit observed experimentally for any metastable state in negative ions.

As there are strong indications that the main cause of beam loss inside the CSR is related to diffusive beam growth, a lifetime extension can be expected if efficient beam cooling can be realized. It is interesting to speculate whether the use of the CSR electron cooler, which in the meantime has been used to cool various atomic and molecular ions, will at some point make it possible to distinguish between the lifetime predictions for the ^2D states, ranging from 9 to 27 h, as given by theoretical calculations for this anion.

ACKNOWLEDGMENTS

This article comprises parts of the doctoral thesis of D.M., to be submitted at the Ruprecht-Karls-Universität Heidelberg, Germany. This work was supported by the Max Planck Society. F.G. and H.K. were supported by the European Research Council under Grant Agreement No. StG 307163. S.S.K. was supported by the Deutsche Forschungsgemeinschaft (DFG) within the DFG Priority Program 1573 "Physics of the Interstellar Medium". X.U. is a Senior Research Associate of the Fonds de la Recherche Scientifique - FNRS, and acknowledges support under Grant No. 4.4504.10.

[1] D. J. Pegg, Rep. Prog. Phys. **67**, 857 (2004).
[2] R. C. Bilodeau and H. K. Haugen, Phys. Rev. Lett. **85**, 534 (2000).
[3] U. Warring, M. Amoretti, C. Canali, A. Fischer, R. Heyne, J. O. Meier, C. Morhard, and A. Kellerbauer, Phys. Rev. Lett. **102**, 043001 (2009).
[4] C. W. Walter, N. D. Gibson, Y.-G. Li, D. J. Matyas, R. M. Alton, S. E. Lou, R. L. Field, D. Hanstorp, L. Pan, and D. R. Beck, Phys. Rev. A **84**, 032514 (2011).
[5] C. W. Walter, N. D. Gibson, D. J. Matyas, C. Crocker, K. A. Dungan, B. R. Matola, and J. Rohlén, Phys. Rev. Lett. **113**, 063001 (2014).
[6] E. Jordan, G. Cerchiari, S. Fritzsche, and A. Kellerbauer, Phys. Rev. Lett. **115**, 113001 (2015).
[7] R. Tang, R. Si, Z. Fei, X. Fu, Y. Lu, T. Brage, H. Liu, C. Chen, and C. Ning, Phys. Rev. A **103**, 042817 (2021).
[8] A. Kellerbauer and J. Walz, New J. Phys. **8**, 45 (2006).
[9] S. M. O'Malley and D. R. Beck, Phys. Rev. A **81**, 032503 (2010).
[10] A. Kellerbauer, A. Fischer, and U. Warring, Phys. Rev. A **89**, 043430 (2014).
[11] G. Cerchiari, A. Kellerbauer, M. S. Safronova, U. I. Safronova, and P. Yzombard, Phys. Rev. Lett. **120**, 133205 (2018).
[12] P. Reinhed, A. Orbán, J. Werner, S. Rosén, R. D. Thomas, I. Kashperka, H. A. B. Johansson, D. Misra, L. Brännholm, M. Björkhage *et al.*, Phys. Rev. Lett. **103**, 213002 (2009).
[13] A. Wolf, K. G. Bhushan, I. Ben-Itzhak, N. Altstein, D. Zajfman, O. Heber, and M. L. Rappaport, Phys. Rev. A **59**, 267 (1999).
[14] U. V. Pedersen, M. Hyde, S. P. Møller, and T. Andersen, Phys. Rev. A **64**, 012503 (2001).
[15] W. C. Martin and R. Zalubas, J. Phys. Chem. Ref. Data **12**, 323 (1983).
[16] P. Andersson, K. Fritioff, J. Sandström, G. Collins, D. Hanstorp, A. Ellmann, P. Schef, P. Lundin, S. Mannervik, P. Royen *et al.*, Phys. Rev. A **73**, 032705 (2006).
[17] E. Bäckström, D. Hanstorp, O. M. Hole, M. Kaminska, R. F. Nascimento, M. Blom, M. Björkhage, A. Källberg, P. Löfgren, P. Reinhed *et al.*, Phys. Rev. Lett. **114**, 143003 (2015).
[18] M. Kamińska, V. T. Davis, O. M. Hole, R. F. Nascimento, K. C. Chartkunchand, M. Blom, M. Björkhage, A. Källberg, P. Löfgren, P. Reinhed *et al.*, Phys. Rev. A **93**, 012512 (2016).
[19] H. T. Schmidt, R. D. Thomas, M. Gatchell, S. Rosén, P. Reinhed, P. Löfgren, L. Brännholm, M. Blom, M. Björkhage, E. Bäckström *et al.*, Rev. Sci. Instrum. **84**, 055115 (2013).
[20] M. K. Kristiansson, S. Schiffmann, J. Grumer, J. Karls, N. de Ruette, G. Eklund, V. Ideböhn, N. D. Gibson, T. Brage, H. Zettergren *et al.*, Phys. Rev. A **103**, 062806 (2021).
[21] R. von Hahn, A. Becker, F. Berg, K. Blaum, C. Breitenfeldt, H. Fadil, F. Fellenberger, M. Froese, S. George, J. Göck *et al.*, Rev. Sci. Instrum. **87**, 063115 (2016).
[22] E. Clementi, A. D. McLean, D. L. Raimondi, and M. Yoshimine, Phys. Rev. **133**, A1274 (1964).
[23] D. Feldmann, Z. Naturforsch. A **26**, 1100 (1971).
[24] A. Kasdan, E. Herbst, and W. C. Lineberger, J. Chem. Phys. **62**, 541 (1975).
[25] M. Scheer, R. C. Bilodeau, C. A. Brodie, and H. K. Haugen, Phys. Rev. A **58**, 2844 (1998).
[26] C. Blondel, C. Delsart, and F. Goldfarb, J. Phys. B: At., Mol. Opt. Phys. **34**, 2757 (2001).

[27] C. Blondel, W. Chaibi, C. Delsart, C. Drag, F. Goldfarb, and S. Kröger, Eur. Phys. J. D **33**, 335 (2005).
[28] W. Chaibi, R. J. Peláez, C. Blondel, C. Drag, and C. Delsart, Eur. Phys. J. D **58**, 29 (2010).
[29] S. M. O'Malley and D. R. Beck, J. Phys. B: At. Mol. Opt. Phys. **36**, 4301 (2003).
[30] C. F. Fischer, G. Gaigalas, P. Jönsson, and J. Bieroń, Comput. Phys. Commun. **237**, 184 (2019).
[31] T. Andersen, Phys. Rep. **394**, 157 (2004).
[32] P. Jönsson, X. He, C. F. Fischer, and I. Grant, Comput. Phys. Commun. **177**, 597 (2007).
[33] S. Fritzsche, Comput. Phys. Commun. **183**, 1525 (2012).
[34] T. Aberg *et al.*, *Corpuscles and Radiation in Matter I,* edited by W. Mehlhorn (Springer-Verlag, Berlin, 1982).
[35] K. Spruck, A. Becker, F. Fellenberger, M. Grieser, R. von Hahn, V. Klinkhamer, O. Novotný, S. Schippers, S. Vogel, A. Wolf *et al.*, Rev. Sci. Instrum. **86**, 023303 (2015).
[36] C. Krantz, O. Novotný, A. Becker, S. George, M. Grieser, R. von Hahn, C. Meyer, S. Schippers, K. Spruck, S. Vogel *et al.*, Nucl. Instrum. Methods, Phys. Rev. A **851**, 92 (2017).
[37] E. Robinson and S. Geltman, Phys. Rev. **153**, 4 (1967).
[38] G. Gribakin, A. Gribakina, B. Gul'Tsev, and V. Ivanov, J. Phys. B: At., Mol. Opt. Phys. **25**, 1757 (1992).
[39] A. P. O'Connor, A. Becker, K. Blaum, C. Breitenfeldt, S. George, J. Göck, M. Grieser, F. Grussie, E. A. Guerin, R. von Hahn *et al.*, Phys. Rev. Lett. **116**, 113002 (2016).
[40] C. Meyer, A. Becker, K. Blaum, C. Breitenfeldt, S. George, J. Göck, M. Grieser, F. Grussie, E. A. Guerin, R. von Hahn *et al.*, Phys. Rev. Lett. **119**, 023202 (2017).
[41] O. Novotný, P. Wilhelm, D. Paul, Á. Kálosi, S. Saurabh, A. Becker, K. Blaum, S. George, J. Göck, M. Grieser *et al.*, Science **365**, 676 (2019).
[42] H. Luna, F. Zappa, M. H. P. Martins, S. D. Magalhães, G. Jalbert, L. F. S. Coelho, and N. V. de Castro Faria, Phys. Rev. A **63**, 052716 (2001).
[43] F. Rahman and B. Hird, At. Data Nucl. Data Tables **35**, 123 (1986).
[44] H. Nishino, S. Clark, K. Abe, Y. Hayato, T. Iida, M. Ikeda, J. Kameda, K. Kobayashi, Y. Koshio, M. Miura *et al.* (Super-Kamiokande Collaboration), Phys. Rev. Lett. **102**, 141801 (2009).
[45] W. B. Cairncross, D. N. Gresh, M. Grau, K. C. Cossel, T. S. Roussy, Y. Ni, Y. Zhou, J. Ye, and E. A. Cornell, Phys. Rev. Lett. **119**, 153001 (2017).
[46] D. H. Lee, W. D. Brandon, D. J. Pegg, and D. Hanstorp, Phys. Rev. A **56**, 1346 (1997).